arXiv:1411.3912v2 [nucl-th] 18 Mar 2015

Systematic Investigation of Negative Cooper-Frye Contributions in Heavy Ion Collisions Using Coarse-grained Molecular Dynamics

D. Oliinychenko,[1, 2, *] P. Huovinen,[1, 3, †] and H. Petersen[1, 3, ‡]

[1] *Frankfurt Institute for Advanced Studies, D-60438 Frankfurt am Main, Germany*
[2] *Bogolyubov Institute for Theoretical Physics, Kiev 03680, Ukraine*
[3] *Institut für Theoretische Physik, Goethe-Universität, D-60438 Frankfurt am Main, Germany*

In most heavy ion collision simulations involving relativistic hydrodynamics, the Cooper-Frye formula is applied to transform the hydrodynamical fields to particles. In this article the so-called negative contributions in the Cooper-Frye formula are studied using a coarse-grained transport approach. The magnitude of negative contributions is investigated as a function of hadron mass, collision energy in the range of $E_{\rm lab}$ = 5–160A GeV, collision centrality and the energy density transition criterion defining the hypersurface. The microscopic results are compared to negative contributions expected from hydrodynamical treatment assuming local thermal equilibrium.

The main conclusion is that the number of actual microscopic particles flying inward is smaller than the negative contribution one would expect in an equilibrated scenario. The largest impact of negative contributions is found to be on the pion rapidity distribution at midrapidity in central collisions. For this case negative contributions in equilibrium constitute 8–13% of positive contributions depending on collision energy, but only 0.5–4% in cascade calculation. The dependence on the collision energy itself is found to be non-monotonous with a maximum at 10-20A GeV.

I. INTRODUCTION

Relativistic hydrodynamics is nowadays the standard approach for modeling ultrarelativistic heavy-ion collisions at highest RHIC (Relativistic Heavy Ion Collider) and LHC (Large Hadron Collider) energies. These dynamical descriptions are either based on ideal [1, 2] or dissipative hydrodynamics [3, 4] and describe the entire expansion fluid dynamically. In so called hybrid approaches [5, 6] only the early hot and dense stage of the expansion is described using hydrodynamics and the later dilute stage by hadron transport.

Most of these models use a conceptually similar procedure: Given an initial condition, the hydrodynamic equations are solved in the whole forward light cone. Near the boundary of vacuum and at the late times of evolution hydrodynamics is not applicable any more, when the density is small and the mean free path is larger than the system size. Therefore, models switch to an off-equilibrium microscopic description in terms of particles in this region. In hybrid approaches particles can scatter, while other models allow only free-streaming and resonance decays. In any case, the most commonly used way to convert the fluid-dynamical fields to particles, a process that we call here 'particlization', is by using the Cooper-Frye formula.

The Cooper-Frye formula assumes particlization to take place on infinitesimally thin three-dimensional hypersurface in four-dimensional space-time. This hypersurface Σ is usually determined a posteriori from hydrodynamical solution in the whole forward light cone, usually as a hypersurface of constant time, energy density, temperature, or Knudsen number. Particle distributions on an infinitesimal element of hypersurface, $d\Sigma$, are calculated using the following formula:

$$p^0 \frac{d^3N}{d^3p} = p^\mu d\sigma_\mu f(p)\,, \tag{1}$$

where $f(p)$ is a distribution function and $d\sigma_\mu$ a normal four-vector of hypersurface with length equal to the area of the infinitesimal surface element. This formula was obtained by Cooper and Frye [7] with the main feature that it respects four-momentum conservation. Though formula (1) is valid for any $f(p)$, the distribution function is usually assumed to be either the boosted thermal distribution $f(p) = f_0(p) = \left[exp\left(\frac{p^\mu u_\mu - \mu}{T}\right) \pm 1\right]^{-1}$ (ideal fluid), or a distribution close to the boosted thermal distribution $f(p) = f_0(p) + \delta f(p)$ (viscous fluid), where $\delta f(p)$ is the dissipative correction. Here T, μ and $u^\mu = \gamma(1, \boldsymbol{v})$ are temperature, chemical potential and the flow velocity of the fluid, respectively.

There is, however, a conceptual problem with the Cooper-Frye formula. Where the surface is space-like, *i.e.*, its normal vector $d\sigma_\mu$ is space-like, and $p^\mu d\sigma_\mu < 0$ for some $\boldsymbol{p}$. Thus if $f(p) > 0$ for all p, as is the case for the thermal distribution, $\frac{d^3N}{d^3p} < 0$ for some $\boldsymbol{p}$. This can be easily seen in the local rest frame of a space-like surface (which always exists since $v_{surf} < c$ for space-like surfaces), where $p^\mu d\sigma_\mu = \boldsymbol{p}\cdot\boldsymbol{n}$ and thus $\frac{d^3N}{d^3p} < 0$ for momenta directed inward the surface. On the other hand, for those time-like surfaces which normal vector points toward the future (*i.e.*, $d\sigma_0 > 0$), $\frac{d^3N}{d^3p} > 0$ for any $\boldsymbol{p}$. This can be also understood as follows: surface is "escaping" faster than the speed of light, so no particle can cross it inward. (For a summary of the properties of time-like and space-like surfaces, see Table I).

If $\frac{d^3N}{d^3p}$ is interpreted as a phase-space density, negative

* oliiny@fias.uni-frankfurt.de
† huovinen@th.physik.uni-frankfurt.de
‡ petersen@fias.uni-frankfurt.de

time-like surface	space-like surface
time-like normal	space-like normal
$d\sigma^\mu d\sigma_\mu > 0$	$d\sigma^\mu d\sigma_\mu < 0$
$v_{surf} > c$	$v_{surf} < c$
$\exists$ RF: $d\sigma^\mu = (\pm dx\, dy\, dz, 0, 0, 0)$	$\exists$ RF: $d\sigma^\mu = (0, 0, 0, dt\, dx\, dy)$
$d\sigma_0 > 0 \Rightarrow \forall p^\mu$: $p^\mu d\sigma_\mu > 0$	$\exists p^\mu$: $p^\mu d\sigma_\mu < 0$
$d\sigma_0 > 0 \Rightarrow \forall p^\mu$: $\frac{d^3N_{CF}}{d^3p} > 0$	$\exists p^\mu$: $\frac{d^3N_{CF}}{d^3p} < 0$

Table I. Properties of surface elements. $g^{\mu\nu} = (1, -1, -1, -1)$. The normal vector is directed toward lower density. RF abbreviates Reference Frame, $\frac{d^3N_{CF}}{d^3p}$ denotes particle distribution from the hypersurface element calculated using the Cooper-Frye formula.

values of it are clearly unphysical, but instead of giving a literal phase-space density, Cooper-Frye formula rather counts the world lines of particles crossing the surface element $d\Sigma$, and gives positive weight to particles moving "outward" and negative weight to particles moving "inward". Thus the negative values of $\frac{d^3N}{d^3p}$, the so-called negative Cooper-Frye contributions, refer to particles flying inward toward the hydrodynamical region, and which should thus be absorbed back to the fluid.

In pure hydrodynamical models, this poses a problem: Particlization takes place at freeze-out when rescatterings cease, and particles stream free. Thus, once particles cross the particlization surface, there is nothing from where particles could scatter back toward the surface, and thus there should be no particles flying back. To avoid this problem, one could choose a completely time-like particlization hypersurface, for example a hypersurface of a constant time without any negative contributions. However, it was shown [8] that particle spectra obtained in such an approach are dramatically different from spectra on a constant temperature hypersurface. Another way is to consider cut-off distribution [9]: $p^0 \frac{d^3N}{dp^3} = p^\mu d\sigma_\mu f(p)\Theta(p^\mu d\sigma_\mu)$. Such a prescription violates conservation laws, unless one adjusts temperature, chemical potentials, and flow velocity in the particle distribution $f(p)$ [10, 11].

On the other hand, there is no such a problem in hybrid models. Particlization takes place where rescatterings are abundant, and thus it is natural to have particles flying back to the fluid-dynamical region. The problem is rather a practical one: What does the negative weight of a particle mean when one samples the particle distributions at particlization surface to create an initial state for the hadron transport? Usually one simply ignores them (see *e.g.* Ref. [12]), which violates conservation laws. An attempt to include these negative weights to the hadron transport was recently made in Ref [13]. Alternatively, if the transition from fluid to transport takes place in a region where hydrodynamics and transport are equivalent, the negative Cooper-Frye contributions coincide with the distribution of particles that backscatter to hydrodynamical region. Thus all one needs to do is to remove these particles from the cascade, but such removing is technically challenging, and the problem remains how to find the region where hydrodynamics and transport lead to equal solutions—assuming that such a region exists at all! Thus the ultimate solution to the problem would be to construct a model, solving coupled hydrodynamical and kinetic equations with the kinetic model providing boundary condition for hydrodynamics. An attempt in this direction was taken by Bugaev [14–16], but these ideas have not yet been implemented in practice.

Fortunately, at high collision energies, the explosive expansion dynamics keeps the negative contributions on the level of a few percent. Emission of particles from time-like areas of surface where no negative contributions appear (so-called volume emission) is much larger than emission from space-like areas (so-called surface emission), and as we will discuss later, large flow velocity reduces negative contributions from space-like surfaces. Nevertheless, there are very few studies that actually quote the values of negative contributions, and investigations at lower collision energies are lacking completely. In this article the negative contributions arising on the Cooper-Frye transition surface assuming distribution functions in local equilibrium are compared to the actual underlying microscopic dynamics to investigate the systematic differences between a transport and a hybrid approach.

Therefore, the aim of the current study is to compare the expected negative contributions in a locally equilibrated hydrodynamical approach with the actual number of particles that scatter back through a hypersurface in a coarse-grained microscopic transport approach. A constant energy density transition surface is constructed and negative Cooper-Frye contributions are compared to actual backscattered particles. In addition, the magnitude of negative contributions is calculated in a systematic way depending on hadron sort, collision energy, centrality, and choice of the transition surface. In Section II the framework for the calculation is explained. Section III shows results of tests of the numerical setup and sensitivity to internal parameters of the calculation. Finally, Section IV contains physical results: the quantification of Cooper-Frye negative contributions and their comparison to backscattered particles.

II. METHODOLOGY

Our calculation is based on the hadronic transport approach - Ultrarelativistic Quantum Molecular Dynamics (UrQMD 3.3p2) [17]. The degrees of freedom in UrQMD are hadrons, resonances up to a mass of 2.2 GeV and strings and the implemented processes include binary elastic and inelastic scatterings which mainly proceed via resonance formation and decays or string excitation and fragmentation at higher collision energies. The UrQMD particles move along classical trajectories and scatter according to their free-particle cross-sections. In our studies there are no long range potentials and particle trajec-

tories between collisions are always straight lines. Using UrQMD we simulate Au + Au collisions at laboratory frame energies $E_{\rm lab}$ = 5, 10, 20, 40, 80 and 160A GeV. This energy region is chosen because we expect UrQMD to provide a reasonable description of the collision dynamics at those energies, and the Cooper-Frye negative contributions to become significant in this energy range.

The general procedure for our calculations is:

1. Generate many UrQMD events and coarse-grain them using a 3+1D space-time grid.
2. Find the local energy density in the Landau rest frame of each grid cell, $\epsilon_{LRF}(t,x,y,z)$, and the collective flow velocity in each cell, $\boldsymbol{v}(t,x,y,z)$.
3. Construct the hypersurface Σ of a constant energy density $\epsilon_{LRF}(t,x,y,z) = \epsilon_c$.
4. Calculate the particle spectra on Σ by using the Cooper-Frye formula and by counting the actual UrQMD particles that cross Σ. To obtain these spectra and to compare them to each other is the goal of the current work.

This procedure mimics switching from hydrodynamics to transport in a hybrid model, but here the "hydrodynamical" picture is obtained by averaging over particle distributions on a space-time grid. Since all the information is still available in the underlying microscopic approach we are able to compare the negative Cooper-Frye contributions to the spectrum of actual backscattered particles. In the following we explain all necessary details for each of these steps of the calculation.

A. Calculating physical quantities on a grid

To obtain the energy density in the Landau rest frame as a function of space-time, that is necessary to construct the Cooper-Frye transition surface, the energy momentum tensor and the net baryon current in the computational frame are calculated

$$T^{\mu\nu}(t,x,y,z) = \frac{1}{\Delta x \Delta y \Delta z} \left\langle \sum \frac{p^\mu p^\nu}{p^0} \right\rangle_N \qquad (2)$$

$$j^\mu_B(t,x,y,z) = \frac{1}{\Delta x \Delta y \Delta z} \left\langle \sum \frac{p^\mu}{p^0} B \right\rangle_N , \qquad (3)$$

where the sum is over all particles in each grid cell at the moment t, and B is the baryon number of each particle. Angular brackets denote averages over N UrQMD events. The cell sizes need to be small enough so that gradients of all relevant physical quantities within the cell are small. On the other hand, if the cell sizes are too small one needs to generate infeasibly many events to damp statistical fluctuations of $T^{\mu\nu}$ components from cell to cell, and obtain a smooth surface Σ. To satisfy these conditions and to ensure energy conservation precisely we choose $\Delta x = \Delta y = 1$ fm, $\Delta z = 0.3$ fm and time step $\Delta t = 0.1$ fm. For the highest collision energy, $E_{\rm lab} = 160A$ GeV, the gradients are larger, so even smaller grid sizes were taken: $\Delta x = \Delta y = 0.3$ fm and $\Delta z = 0.1$ fm. This choice is further discussed in the Section III, where the sensitivity of results to the grid size is studied. Since even $N = 10\,000$ events do not provide enough statistics to obtain a smooth hypersurface, and increase of N is not feasible due to limited storage capacities, the individual particles are smeared by marker particles distributed according to a Gaussian distribution.

Every UrQMD particle with coordinates (t_p, x_p, y_p, z_p) and four-momentum p^μ is substituted by N_{split} particles with coordinates distributed with probability density $f(x,y,z) \sim \exp\left(-\frac{(x-x_p)^2}{2\sigma^2} - \frac{(y-y_p)^2}{2\sigma^2} - \gamma_z^2 \frac{(z-z_p)^2}{2\sigma^2}\right)$, where $\gamma_z = (1 - p^z/p^0)^{-1/2}$. These marker particles are attributed the 4-momentum and quantum numbers of the original particle divided by N_{split}. In our calculation $N_{split} = 300$ and $\sigma = 1$ fm. The sensitivity of our results to the width of the Gaussian is discussed in Section III. When this Gaussian smearing is applied, stable results are obtained with only $N = 1500$ events, which we employ for our calculations.

B. The hypersurface construction

After obtaining $T^{\mu\nu}$ in the computational frame, it has to be transformed to the Landau rest frame (LRF) in each cell. By definition, $T^{0i}_{LRF} = 0$, *i.e.*, the energy flow in the LRF is zero. To find the LRF we solve the generalized eigenvalue problem $(T^{\mu\nu} - \lambda g^{\mu\nu})h_\nu = 0$. The eigenvector corresponding to the largest eigenvalue is proportional to the 4-velocity of the LRF and the proportionality constant is fixed by the constraint that $\sqrt{u_\mu u^\mu} = 1$. After finding $T^{\mu\nu}_{LRF}$ the hypersurface of constant Landau rest frame energy density is constructed where $T^{00}_{LRF} \equiv \epsilon_{LRF}(t,x,y,z) = \epsilon_c$, with ϵ_c a parameter that characterizes the hypersurface. In such a way we mimic the transition surface in hybrid models, which typically use ϵ_c = 0.3–1 GeV/fm^3 [12]. The isosurface is constructed using the Cornelius subroutine [12], that provides a continuous surface without holes and avoids double counting of hypersurface pieces. The subroutine provides the normal four-vectors $d\sigma_\mu$ of the hypersurface. The physical quantities on the grid, *i.e.*, the energy, net baryon density and the flow velocity, are linearly interpolated to the geometrical centers of the hypersurface elements.

C. Thermodynamic quantities

To apply the Cooper-Frye formula one needs the temperature T and chemical potentials on the surface, which do not exist in the microscopic picture. Strictly speaking they make sense only in the vicinity of thermal and chemical equilibrium, which may not be the case in our

UrQMD simulation. Nevertheless, we take the LRF energy density and net baryon density to mean equilibrium densities—as is the case when deviations from equilibrium are small—and obtain temperature and chemical potentials from an ideal hadron resonance gas (HRG) equation of state (EoS) containing the same hadrons and resonances as UrQMD. Since our EoS assumes zero strangeness density, we impose this constraint as well, even if UrQMD itself allows local non-zero strangeness. In practice, this means solving the following coupled equations to find the temperature T, baryon chemical potential μ_B and strangeness chemical potential μ_S:

$$\epsilon_{LRF} = \sum_p \frac{g_p}{(2\pi)^3} \int \frac{d^3k\,\sqrt{k^2+m^2}}{e^{(\sqrt{k^2+m_p^2}-\mu_B B_p-\mu_S S_p)/T}\pm 1} \quad (4)$$

$$n_B^{LRF} = \sum_p \frac{g_p B_p}{(2\pi)^3} \int \frac{d^3k}{e^{(\sqrt{k^2+m_p^2}-\mu_B B_p-\mu_S S_p)/T}\pm 1} \quad (5)$$

$$n_S^{LRF} = \sum_p \frac{g_p S_p}{(2\pi)^3} \int \frac{d^3k}{e^{(\sqrt{k^2+m_p^2}-\mu_B B_p-\mu_S S_p)/T}\pm 1} \quad (6)$$

Here $\epsilon_{LRF} = T^{00}$ is the energy density in LRF, n_B^{LRF} is the baryon density in LRF, n_s is the strangeness density, and the sum runs over all hadron species that appear in UrQMD; m_p is the mass of a hadron p, g_p is its spin and isospin degeneracy factor, and B_p and S_p are its baryon number and strangeness, respectively.

D. Cooper-Frye and "by particles" calculations

After the hypersurface of constant LRF energy density Σ is obtained and T and μ are evaluated using the EoS, the Cooper-Frye formula is applied on the hypersurface. The spectrum from the Cooper-Frye formula is split into positive and negative parts:

$$\frac{dN_{CF}^{+}}{p_T dp_T d\varphi dy} = \frac{g}{(2\pi)^3} \int_\sigma \frac{\Theta(p^\mu d\sigma_\mu)\, p^\mu d\sigma_\mu}{e^{(p^\nu u_\nu-\mu)/T}\pm 1} \quad (7)$$

$$\frac{dN_{CF}^{-}}{p_T dp_T d\varphi dy} = \frac{-g}{(2\pi)^3} \int_\sigma \frac{\Theta(-p^\mu d\sigma_\mu)\, p^\mu d\sigma_\mu}{e^{(p^\nu u_\nu-\mu)/T}\pm 1} \quad (8)$$

To evaluate dN/dy or $dN/p_T dp_T$ the integrations are performed numerically, applying the 36×36 points Gauss-Legendre method to integrals transformed to finite limits.

For comparison with the Cooper-Frye calculation we count the actual microscopic (not marker) particles crossing the same hypersurface Σ that is used for Cooper-Frye calculations. Inward and outward crossings are counted separately. To find the point, where a particle trajectory crosses Σ we use the fact that by construction the energy density $\epsilon > \epsilon_c$ inside the surface and $\epsilon < \epsilon_c$ outside of it. The energy density is interpolated to the particle trajectory to find the point where $\epsilon - \epsilon_c$ changes sign. Each of these crossings is counted as positive, if the particle streams outward and negative, if the particle flies toward higher energy densities.

Both Cooper-Frye calculation and particle counting start at the same time t_{start}, which depends on the collision energy. Following the prescription from hybrid models, we take $t_{start} = \frac{2R}{v\gamma}$. This is the time two nuclei need to pass through each other. Numerical values are 8 fm/c for 5A GeV, 5.6 fm/c for 10A GeV, 4 fm/c for 20A GeV, 2.8 fm/c for 40A GeV, 2 fm/c for 80A GeV and 1.4 fm/c for 160A GeV. The same t_{start} is used for all centralities.

III. SENSITIVITY TO INTERNAL PARAMETERS AND FULFILLMENT OF CONSERVATION LAWS

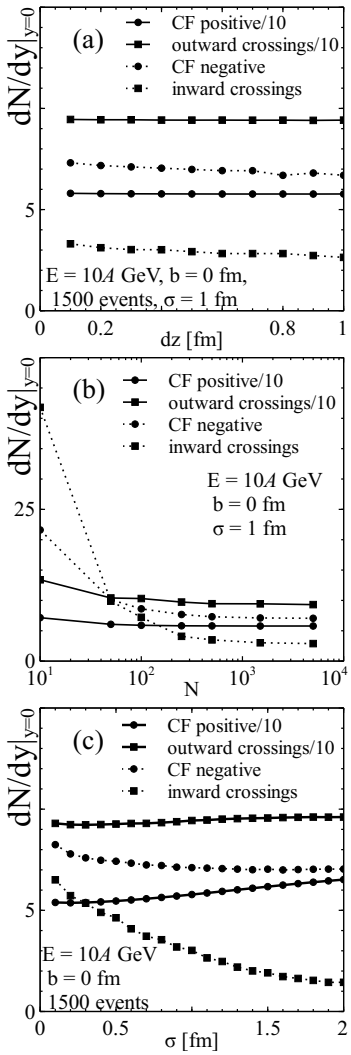

Figure 1. Sensitivity of results to internal parameters of the simulation: grid spacing along z axis, dz (a), number of events, N (b) and the width σ of Gaussian smearing (c).

Besides physical parameters like the beam energy, $E_{\rm lab}$, and centrality of the collision controlled by the impact parameter b, our simulation contains internal parameters like grid spacing, the width of the smearing Gaussian σ,

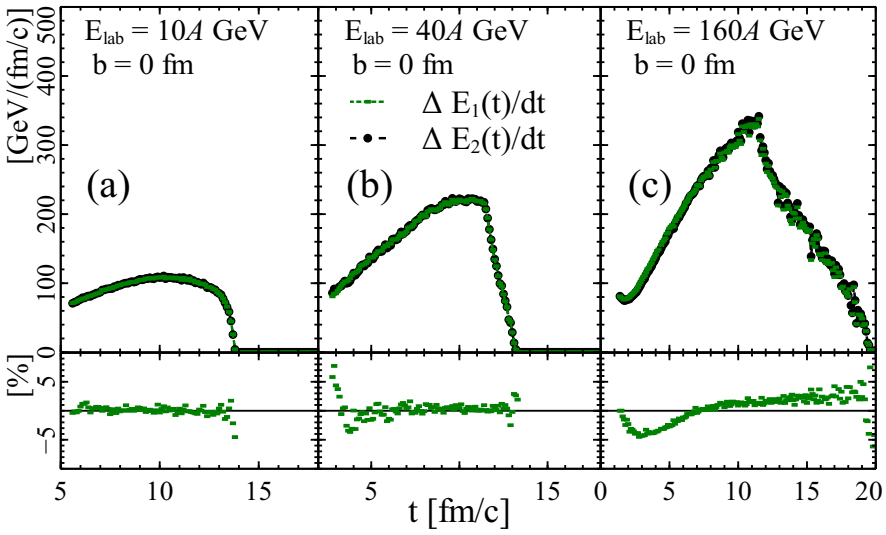

Figure 2. (Color online) Energy flux through the surface at different times evaluated as actual flow, $\Delta E_1(t)/dt = \int_{t-dt}^{t} T^{\mu 0} d\sigma_\mu/dt$ (circles), and as a difference in energy within the surface at different times, $\Delta E_2(t)/dt = (E_{in}(t) - E_{in}(t-dt))/dt$ (rectangles). Lower panel shows the relative difference between these two measures in %, and thus the conservation of energy in the calculation.

and the number of events N. Ideally, we should work in such a region of internal parameters, that our results are independent of them. To see how sensitive our results are to these internal parameters, the positive and negative contributions to the pion yield at midrapidity, $\frac{dN}{dy}|_{y=0}$, at different values of these parameters are evaluated.

The calculation is more sensitive to the grid spacing in z direction, dz, than to the spacings in x and y directions, dx and dy, since gradients of $T^{\mu\nu}$ are largest in the longitudinal direction. Although, as shown in Fig. 1 a), even the sensitivity to dz is weak over a reasonable range of values. The main motivation for choosing the grid spacing and time step comes in fact from the requirement of energy conservation discussed later.

The results are very sensitive to the small number of events (see Fig. 1 b), but already $N = 500$ events provides sufficient statistics for stable results. To be on the safe side, we have analyzed $N = 1500$ events for our final results. Unfortunately, our results are not completely independent of the width σ of the Gaussian smearing, as shown on Fig. 1 c). The number of inward crossing UrQMD pions is most sensitive to σ. Two effects play a role here: at small σ the surface still has large statistical fluctuations and small scale structures, "lumps" (See Fig. 2 of Ref [18]), whereas at large σ Gaussian smearing pushes transition surface further out in space. Further out the densities are smaller, and the UrQMD particle distributions are further away from equilibrium so that especially the number of particles moving toward the center is strongly reduced. We choose $\sigma = 1$ fm as a reasonable value for our calculations, but keep in mind that varying σ in the range from 0.6 fm to 1.4 fm causes ~ 20 % difference in the number of inward crossings. We consider this a systematic error in our analysis, but fortunately this uncertainty does not affect our main conclusions.

To check that energy is conserved in the coarse-graining procedure, we evaluate the energy flow through the surface during the time step dt, $\Delta E_1(t) = \int_{t-dt}^{t} T^{\mu 0} d\sigma_\mu$, and compare it to the change in energy within the surface during the same time step, $\Delta E_2(t) = E_{in}(t) - E_{in}(t - dt)$, where E_{in} is total energy of particles inside the surface. Ideally $\Delta E_1(t) = \Delta E_2(t)$ for any dt, but finite cell sizes limit the precision and break the conservation of energy. The accuracy of $\Delta E_1 \approx \Delta E_2$ improves when grid spacing and time step are decreased. Fig. 2 shows the energy flux through the surface and the relative difference between $\Delta E_1(t)$ and $\Delta E_2(t)$ in central collisions at energies $E_{\rm lab} = 10, 40, 160A$ GeV. To achieve better than 5% percent accuracy at all times, we use small grid spacing with $\Delta x = \Delta y = 1$ fm, $\Delta z = 0.3$ fm, and time step $\Delta t = 0.1$ fm/c in collisions with $E_{\rm lab} \leq 80A$ GeV, and even finer grid with $\Delta x = \Delta y = 0.3$ fm, and $\Delta z = 0.1$ fm for collisions at $E_{\rm lab} = 160A$ GeV. When integrated over the whole collision time, the violation of energy conservation is less than 1% at all collision energies. We have done a similar check for the net baryon charge, and obtained similar results.

IV. RESULTS AND DISCUSSION

Let us start by investigating the properties of the transition hypersurface itself as a function of beam energy. Figure 3 depicts the surface Σ in longitudinal direction along the x axis. We see that with increasing energy, the lifetime of the system increases. This indicates longer lasting surface emission (from space-like parts of the sur-

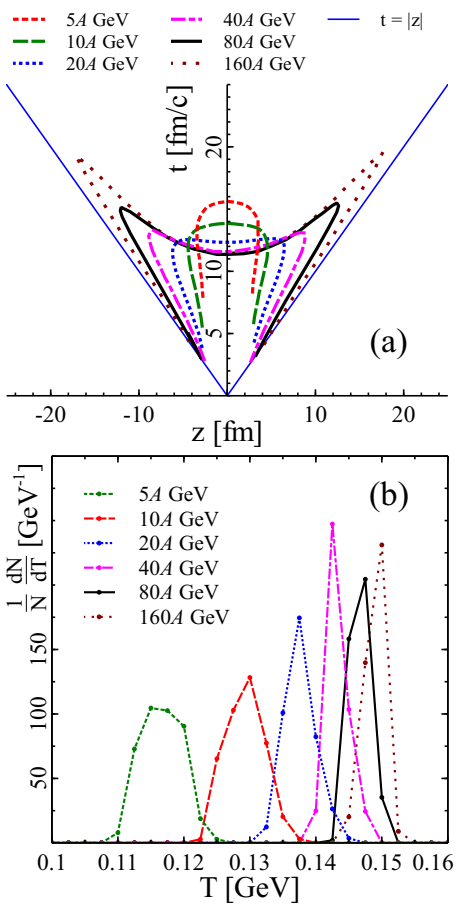

Figure 3. (Color online) Upper panel: Hypersurface of constant LRF energy density $\epsilon(t,0,0,z) = \epsilon_c = 0.3$ GeV/fm^3. Lower panel: The fraction of hypersurface elements with (apparent) temperature T in central Au+Au collisions at the collision energy of $E_{\rm lab} = 5$, 10, 20, 40, 80, 160A GeV.

face), which might lead to larger negative contributions. On the other hand, with increasing energy the longitudinal expansion leads to larger volume of the final volume emission (from time-like parts of the surface), which indicates smaller negative contributions. Thus we have two competing effects, and one has to carry out the actual calculation to find out how the negative contributions depend on energy.

Distributions of the (apparent) temperature of the hypersurface elements are shown on the right panel of Fig. 3. At each collision energy temperature distribution is rather narrow, which means that constant energy density surface approximately coincides with constant temperature surface. As well, the average temperature increases with increasing collision energy as expected from thermal model fits to particle yields [19].

In Fig. 4 we compare rapidity spectra of identified particles in $E_{\rm lab} = 40A$ GeV Au+Au collisions obtained by Cooper-Frye calculation and by counting of the microscopic particles. Even though, we are showing the results only for one collision energy, all results are qualitatively the same at all other energies. If UrQMD is close to equilibrium on a surface at $\epsilon_c = 0.3$ GeV/fm^3, both approaches should yield similar distributions. At midrapidity this is the case for nucleons, and with a lesser accuracy for kaons. Δ's, Λ's, ρ's and η's which are not shown in the figure depict a behavior similar to nucleons. However, the pion yields are wildly different indicating that pions are—and thus the entire system is—far away from chemical equilibrium at least. To cancel the effect of non-equilibrium and to make the differences in momentum distributions visible we consider not the absolute value of the negative contributions, but the ra-

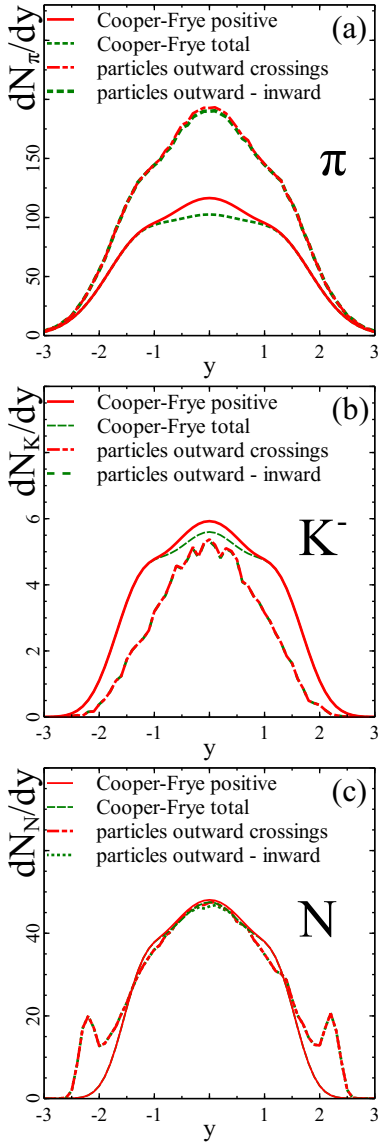

Figure 4. (Color online) Rapidity distribution of identified particles obtained from Cooper-Frye formula on the surface Σ and from explicit counting of particles that cross the same surface. Positive contributions and the net distribution, *i.e.*, positive-negative, are shown separately. $E_{\rm lab} = 40A$ GeV, central Au+Au collisions.

tio of negative to positive ones, $(dN^-/dy)/(dN^+/dy)$ or $(dN^-/dp_T)/(dN^+/dp_T)$. From Fig. 4 it is also apparent that the magnitude of the negative contributions is always small compared to the positive ones as expected.

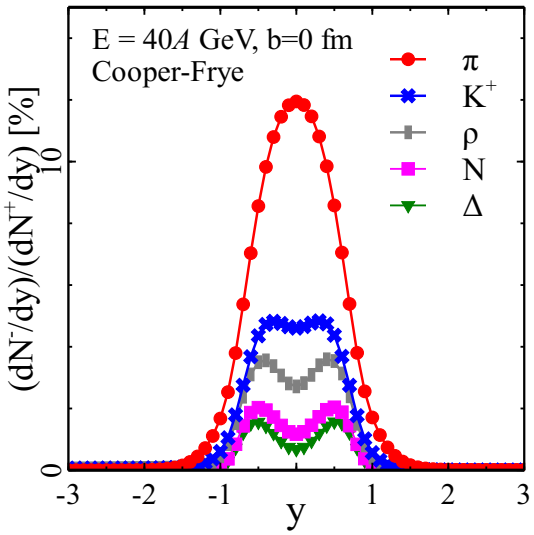

Figure 5. (Color online) Rapidity distribution of the ratio of negative to positive contributions for different hadron species: pions (circles), K^+ (crosses), ρ (bars), nucleons (rectangles), and deltas (triangles). Cooper-Frye calculation in central Au+Au collisions at $E_{\rm lab} = 40A$ GeV.

The dependence of the ratio $(dN^-/dy)/(dN^+/dy)$ on the hadron type is illustrated in Fig. 5 by the Cooper-Frye results. Since for all cases, the microscopic negative contributions of backstreaming particles are much smaller than the Cooper-Frye ones we concentrate on showing the maximal effect. Surface temperature and velocity profiles are identical for all hadrons, so the plot demonstrates first of all the effect of particle mass. One can see that the average value of $(dN^-/dy)/(dN^+/dy)$ decreases with particle mass. This can be understood by considering a small volume of fluid in its rest frame, and a space-like surface moving through it with a velocity $0 < v_{surf} < c$ so that lower density, *i.e.*, outside, is in the negative direction. To be counted as a negative contribution, a particle must enter the fluid, and thus have a larger velocity than the surface. Average thermal velocity decreases with increasing mass, and therefore the heavier the particle, the fewer of them cross the surface inward. Since relative negative contributions for pions are several times larger than for other hadrons we will consider only pions in the following.

As could be seen in Fig. 4, imposing equilibrium for Cooper-Frye calculation leads to significantly larger negative to positive contribution ratio at midrapidity than the counting of UrQMD particles. As shown in Fig. 6 this holds for all the energies we have considered, showing that the system is out of not only chemical, but also of kinetic equilibrium. Either the collective flow velocity of pions is different from the collective velocity of

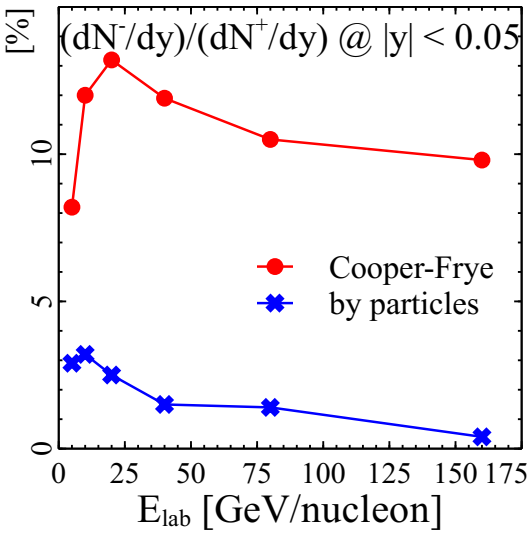

Figure 6. (Color online) The ratio of negative to positive contributions on the $\epsilon(t,x,y,z) = \epsilon_c = 0.3$ GeV/fm^3 surface for pions at midrapidity in central Au+Au collisions at various collision energies. Circles depict Cooper-Frye result and rectangles the explicit counting of UrQMD particles.

other particles [20, 21] or the dissipative corrections to pion distribution are very large. We have also checked that the relative microscopic negative contributions are much smaller in UrQMD at all centralities, for all particle species, and on isosurfaces of energy density $\epsilon_c = 0.3$ and 0.6 GeV/fm^3.

On the other hand, the trend as a function of collision energy in Cooper-Frye and UrQMD calculations is the same: both curves have a maximum at 10-20A GeV and then decrease with increasing energy. This behavior is a result of a complicated interplay of several factors: temperature, relative velocities between surface and fluid, and relative amounts of volume and surface emission, *i.e.*, emission from the time- and space-like parts of the surface. To gain some insight we consider all these factors separately. The same argument used to explain the sensitivity of negative contributions to particle mass, explains why larger temperature leads to larger negative contributions. Temperature on the constant density surface grows with increasing collision energy (see Fig. 3), which would lead one to expect an increase of negative contributions with increasing collision energy. On the other hand, larger relative velocity between the fluid and surface reduces the negative contributions (again the same argument), and we see that the average relative velocity increases with increasing collision energy. Finally, as argued when discussing Fig. 3, we have seen that the larger the collision energy, the larger the fraction of volume emission. Which, as mentioned, reduces the negative contributions.

It is instructive to evaluate the negative contributions as function of transverse momentum p_T as well, as shown in Fig. 7 for Cooper-Frye calculation and "by particles".

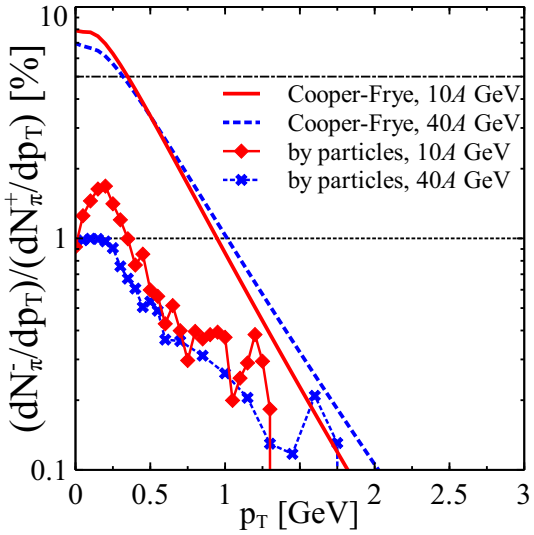

Figure 7. (Color online) The ratio of negative to positive pion contributions as a function of transverse momentum at midrapidity in central Au+Au collisions at $E_{\rm lab}$ = 5, 10, 20, 40, 80A GeV.

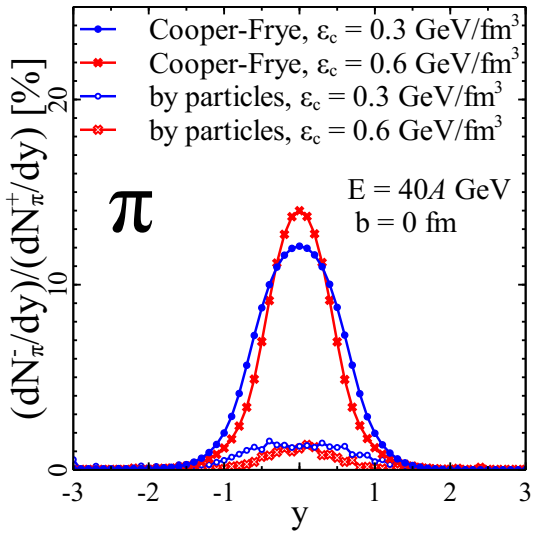

Figure 8. (Color online) Rapidity distribution of the ratio of negative to positive contributions for pions on $\epsilon(t,x,y,z) = \epsilon_c = 0.3$ GeV/fm^3 (circles) and $\epsilon_c = 0.6$ GeV/fm^3 (crosses) surfaces in central Au+Au collisions at $E_{\rm lab}$ = 40 A GeV. Full symbols correspond to Cooper-Frye calculation and open symbols to explicit counting of UrQMD particles.

One can see that the largest negative contributions are located at small p_T, which means that one can reduce the uncertainty caused by the negative contributions by a low p_T cut. Also as a function of transverse momentum, the amount of microscopically backward streaming particles is much smaller than in an equilibrium scenario.

When discussing Fig. 6 we mentioned that, independent of the energy density of the surface, the negative contributions are much smaller when counting the UrQMD particles. Furthermore, in Cooper-Frye calculations the strength of the negative contributions depends on the value of ϵ_c where the distributions are evaluated as shown in Fig. 8. Larger ϵ_c leads to larger negative contribution at midrapidity and lower at back- and forward rapidities. This result arises from interplay of two factors: larger temperature and smaller average v_{rel} for larger energy density. Quite surprisingly the negative contributions evaluated by counting the UrQMD particles is almost independent of the value of ϵ_c. This indicates that even in much higher temperature $T \sim 155$–160 MeV the microscopic system is not fully thermalised.

Dependence of the contribution ratio on centrality is shown in Fig. 9. The negative contributions decrease with decreasing centrality because the more peripheral the collision, the larger the fraction of time-like hypersurface elements. This behavior is illustrated in the right panel of Fig. 9. In the limit of very peripheral collisions the lifetime of the system becomes zero, and thus the surface is time-like everywhere and there are no negative contributions at all. Temperature and relative velocities appear to be less important factors in this case than relative amount of time-like and space-like hypersurface elements.

Let us finally compare our results to previous studies. In [12] negative contributions were evaluated on the $\epsilon = 0.3$ GeV/fm^3 transition surface of a hybrid model at SPS and RHIC energies—$E_{\rm lab} = 160A$ GeV and $\sqrt{s_{\rm NN}} = 200$ GeV, respectively—and found to be around $(dN_\pi^-/dy)/(dN_\pi^+/dy) \simeq 13\%$ and 9% at $y = 0$. The negative contributions for 160A GeV are slightly larger than in our calculation. The reason for this discrepancy lies in the difference of the velocity profiles on the hypersurfaces: In hydrodynamics the average relative velocity between flow and surface is smaller than in our transport-based approach, which leads to larger negative contributions.

V. CONCLUSIONS

We have investigated negative Cooper-Frye contributions and backscattering using a coarse-grained molecular dynamics approach. Au+Au collisions at $E_{\rm lab}$ = 5–160 A GeV energies have been simulated using UrQMD, and a hypersurface Σ of constant Landau rest frame energy density has been constructed. On this surface we have calculated two quantities: The ratio of Cooper-Frye negative to positive contributions, which assumes local thermal equilibrium, and the ratio of UrQMD particles crossing Σ inward to crossing Σ outward, which assumes no equilibrium.

We found that at all collision energies the ratio of inward to outward moving particles calculated counting the UrQMD particles is much smaller than the same ratio calculated assuming equilibrium, *i.e.*, the Cooper-Frye negative to positive ratio. This finding poses a question

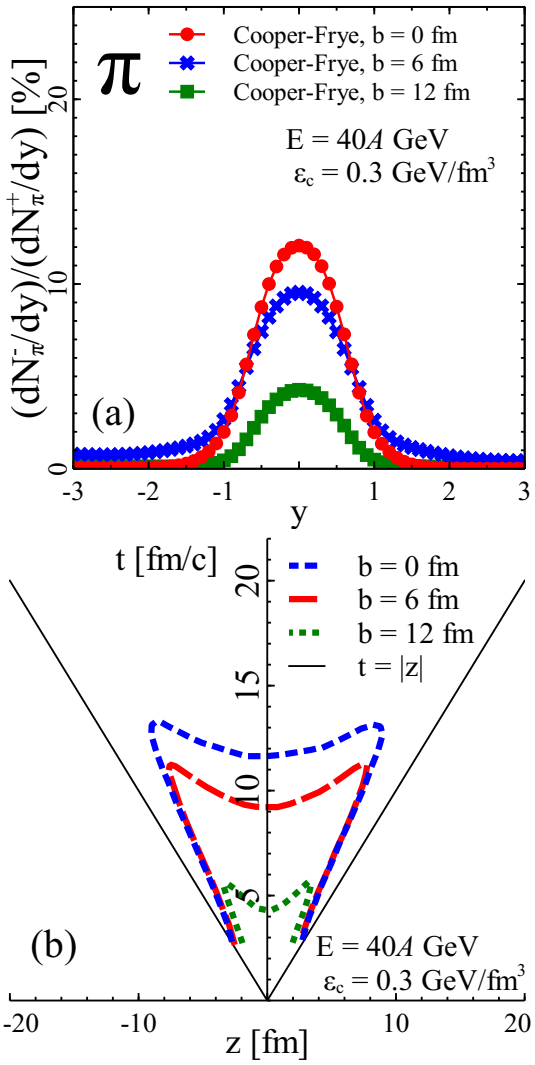

Figure 9. (Color online) Upper panel: Rapidity distribution of the ratio of negative to positive contributions for pions in Au+Au collisions at $E_{\rm lab} = 40$ A GeV at various centralities: $b = 0$ (circles), $b = 6$ fm (crosses) and $b = 12$ fm (rectangles). Lower panel: hypersurfaces along the z axis in the same collisions at the same centralities.

to the construction of hybrid models, and the treatment of freeze-out in hydrodynamical models: If the cascade leads to distributions nowhere near equilibrium, how are the hydrodynamical and cascade stages to be connected in a consistent fashion? On the other hand, this result shows that an ideal fluid dynamics hybrid approach contains the worst case scenario for negative contributions and even then they are on the order of max. 15% for the pion yield at midrapidity. What remains to be seen, however, is whether we could get closer to the UrQMD result if we allowed dissipative corrections to the distribution function of Cooper-Frye, or whether the deviations from equilibrium are so large that dissipative expansion is not feasible.

The largest observed impact of negative contributions is to pion rapidity spectrum at midrapidity in central collisions. In thermally equilibrated Cooper-Frye calculations it constitutes 8–13%, but only 0.5–4% in the counting of UrQMD particles. The Cooper-Frye value roughly agrees with the values obtained previously for hydrodynamics at 160 GeV. We found several systematic features in these ratios. They are smaller for larger hadron mass and therefore largest for pions. The relative negative contributions decrease as a function of collision energy and by going from central to peripheral collisions. On the other hand, they increase if a higher energy density is chosen as a surface criterion. The small scale structures on the surface, its "lumpiness", play a significant role: If the surface is not smooth enough both ratios can increase dramatically. Therefore, an interesting future study could be to compare single fluctuating events to the averaged result.

ACKNOWLEDGMENTS

This work was supported by the Helmholtz International Center for the Facility for Antiproton and Ion Research (HIC for FAIR) within the framework of the Landes-Offensive zur Entwicklung Wissenschaftlich-Oekonomischer Exzellenz (LOEWE) program launched by the State of Hesse. DO and HP acknowledge funding of a Helmholtz Young Investigator Group VH-NG-822 from the Helmholtz Association and GSI, and PH by BMBF under contract no. 06FY9092. Computational resources have been provided by the Center for Scientific Computing (CSC) at the Goethe University of Frankfurt.

[1] P. F. Kolb and U. Heinz, in *Quark-Gluon Plasma 3*, edited by R. C. Hwa and X.-N. Wang (World Scientific, Singapore, 2004), p. 634.
[2] P. Huovinen and P. V. Ruuskanen, Ann. Rev. Nucl. Part. Sci. **56**, 163 (2006).
[3] U. W.Heinz and R. Snellings, Annu. Rev. Nucl. Part. Sci. **63**, 123 (2013).
[4] C. Gale, S. Jeon and B. Schenke, Int. J. Mod. Phys. A **28**, 1340011 (2013).
[5] T. Hirano, P. Huovinen, K. Murase and Y. Nara, Prog. Part. Nucl. Phys. **70**, 108 (2013).
[6] H. Petersen, arXiv:1404.1763 [nucl-th].
[7] F. Cooper and G. Frye, Phys. Rev. D **10**, 186 (1974).
[8] D. H. Rischke, Lect. Notes Phys. **516**, 21 (1999).
[9] K. A. Bugaev, Nucl. Phys. A **606**, 559 (1996).
[10] C. Anderlik, Z. I. Lazar, V. K. Magas, L. P. Csernai, H. Stoecker and W. Greiner, Phys. Rev. C **59**, 388 (1999).
[11] C. Anderlik *et al.*, Phys. Rev. C **59**, 3309 (1999).
[12] P. Huovinen and H. Petersen, Eur. Phys. J. A **48**, 171 (2012).

[13] S. Pratt, Phys. Rev. C **89**, 024910 (2014).
[14] K. A. Bugaev and M. I. Gorenstein, nucl-th/9903072.
[15] K. A. Bugaev, Phys. Rev. Lett. **90**, 252301 (2003).
[16] K. A. Bugaev, Phys. Rev. C **70**, 034903 (2004).
[17] S. A. Bass *et al.*, Prog. Part. Nucl. Phys. **41** (1998) 255; M. Bleicher *et al.*, J. Phys. G G **25** (1999) 1859.
[18] P. Huovinen, M. Belkacem, P. J. Ellis and J. I. Kapusta, Phys. Rev. C **66**, 014903 (2002).
[19] A. Andronic, P. Braun-Munzinger and J. Stachel, Phys. Lett. B **673**, 142 (2009).
[20] H. Sorge, Phys. Lett. B **373**, 16 (1996).
[21] S. Pratt and J. Murray, Phys. Rev. C **57**, 1907 (1998).